Petroleum Science 20 (2023) 1238–1246

Contents lists available at ScienceDirect

Petroleum Science

journal homepage: www.keaipublishing.com/en/journals/petroleum-science

Original Paper

Influences of pore fluid on gas production from hydrate-bearing reservoir by depressurization

Yi-Fei Sun [a, b], Bo-Jian Cao [a], Hong-Nan Chen [a], Yin-Long Liu [a], Jin-Rong Zhong [c], Liang-Liang Ren [d], Guang-Jin Chen [a, *], Chang-Yu Sun [a], Dao-Yi Chen [b, **]

[a] State Key Laboratory of Heavy Oil Processing, China University of Petroleum, Beijing 102249, China
[b] Division of Ocean Science and Technology, Tsinghua Shenzhen International Graduate School, Tsinghua University, Shenzhen, Guangdong 518055, China
[c] School of Chemistry and Food Engineering, Changsha University of Science & Technology, Changsha, Hunan 410114, China
[d] Oilfield Chemicals R&D Institute, COSL, Hebei 065201, China

ARTICLE INFO

Article history:
Received 16 April 2022
Received in revised form
2 August 2022
Accepted 15 September 2022
Available online 20 September 2022

Edited by Jia-Jia Fei

Keywords:
CH_4 hydrate
Water saturation
Depressurization
Gas-phase space
N_2 sweep

ABSTRACT

In addition to the temperature and pressure conditions, the pore fluid composition and migration behavior are also crucial to control hydrate decomposition in the exploitation process. In this work, to investigate the effects of these factors, a series of depressurization experiments were carried out in a visible one-dimensional reactor, using hydrate reservoir samples with water saturations ranging from 20% to 65%. The results showed a linear relationship between gas production rates and gas saturations of the reservoir, suggesting that a larger gas-phase space was conducive to hydrate decomposition and gas outflow. Therefore, the rapid water production in the early stage of hydrate exploitation could release more gas-phase space in the water-rich reservoir, which in turn improved the gas production efficiency. Meanwhile, the spatiotemporal evolution of pore fluids could lead to partial accelerated decomposition or secondary formation of hydrates. In the unsealed reservoir, the peripheral water infiltration kept reservoir at a high water saturation, which hindered the overall production process and caused higher water production. Importantly, depressurization assisted with the N_2 sweep could displace the pore water rapidly. According to the results, it is recommended that using the short-term N_2 sweep as an auxiliary means in the early stage of depressurization to expand the gas-phase space in order to achieve the highest production efficiency.

1. Introduction

Natural gas hydrates (NGHs) are nonstoichiometric crystalloid compounds that are formed from water (the host) and small gas molecules (the guest) under low temperature and high pressure conditions (Sloan, 2003; Ning et al., 2012; Cui et al., 2019). NGHs resources discovered so far are widely distributed in the submarine sediments-bound reservoir on continental margins and permafrost regions (Boswell and Collett, 2011), the total amount of which is twice as much as the other conventional energy sources combined (Makogon, 2010). Due to the all-round advantages of wide distribution, huge reserves and being methane-based clean energy (Sloan and Koh, 2007), NGHs are considered as a promising alternative energy resource and have become a hot research topic in the world (Chong et al., 2016; Zhou et al., 2019).

Fundamentally differing from the development of traditional oil and gas resources (Hu et al., 2014), the naturally forming solid hydrates first *in situ* decompose into flowable gas and water, and then the gas is produced and collected. That is to say, the recovery efficiency of NGHs is jointly controlled by hydrate decomposition rate and gas production rate. Now the well-explored methods for hydrate decomposition include depressurization (Li et al., 2010; Yang et al., 2012; Chong et al., 2017), heat stimulation (Yang et al., 2010; Wang et al., 2013; Li et al., 2018), inhibitor injection (Yuan et al., 2011, 2013; Cha et al., 2013) and gas sweep (Wang et al., 2015; Sun et al., 2018a). Specifically, depressurization and heat stimulation directly shift the pressure and temperature conditions of hydrate reservoir, while the mechanisms of inhibitor injection

* Corresponding author.
** Corresponding author.
E-mail addresses: gjchen@cup.edu.cn (G.-J. Chen), chen.daoyi@sz.tsinghua.edu.cn (D.-Y. Chen).

https://doi.org/10.1016/j.petsci.2022.09.015

and gas sweep are changing the hydrate phase equilibrium conditions. Considering the economy and operability of the depressurization method, the combination methods based on depressurization with the heat/inhibitor/gas/water injection as auxiliary means have been applied to achieve more efficient gas production (Dou et al., 2009; Feng et al., 2016; Nair et al., 2018; Sun et al., 2018b, 2021). Additionally, the depressurization based methods have also been applied to several field trials (Dallimore et al., 2005; Konno et al., 2017; Chen et al., 2018; Wei et al., 2021), and the quantities of gas production as well as the rates have been gradually increased as the maturity of mining technology and equipment. On the whole, hydrate decomposition mainly involves two controlling factors, mass transfer and heat transfer. Timely releasing the pore fluid is the key to maintaining a high driving force during depressurization. The uncertainty associated with reservoir parameters and their impact on key production response were analyzed (Aghajari et al., 2019). On the other hand, many studies have proven that the production efficiency is controlled by heat transfer after the reduction of reservoir pressure (Yang et al., 2012; Li et al., 2016, 2019). Heat injection can fill up the heat difference to some extent which is caused by the endothermic decomposition of gas hydrate, but the energy efficiency is unsatisfactory due to the inevitable heat waste in the sediments (Kurihara et al., 2009). In order to alleviate the temperature effect caused by hydrate decomposition, the optimization strategies, such as multi-stage depressurization (Wang et al., 2020; Gao et al., 2021), cyclic depressurization (Konno et al., 2016), and depressurization below quadruple point (Wang et al., 2016), etc., have been proposed in recent years. However, these methods have been proven to have negative effect on the gas production rate. In addition, CO_2—CH_4 replacement can also maintain the reservoir temperature (Yuan et al., 2012; Sun et al., 2021), but the low replacement efficiency of gas replacement method cannot be neglected. Therefore, the heat transfer behavior during hydrate exploitation is still focused by researchers. In a practical production process, the multiphase fluid flow in reservoir has a huge impact on the heat transfer. Hydrate exploitation is not only to effectively stimulate hydrate decomposition, but also to rapidly produce the released gas. However, researches on the multiphase flow during hydrate decomposition in unsealed water-rich reservoirs are relatively inadequate. Therefore, we started to explore the effect of pore water saturation and peripheral water infiltration on the hydrate decomposition, which is important for the selection and optimization of mining methods.

Recently, the studies on gas production have focused more on the water-saturated hydrate reservoir to simulate the marine hydrate resources development. Wang et al. (2018) compared the hydrate decomposition by depressurization and heat stimulation at the initial water saturation of 20% and 67.5% in a pilot scale simulator. The results indicated the significant influence of the pore water on fluid flow and heat transfer. Gas flow channels were necessary to discharge the released gas, while the excess pore water in turn hindered the gas transfer. Chong et al. (2017) studied the effect of production pressure on gas production at an initial water saturation of ~50%. Importantly, sub-freezing mining can achieve higher cumulative gas production and lower water production. However, for the NGHs occurrence conditions in the South China Sea, it is too difficult to reduce the reservoir temperature below the freezing point. Additionally, the decreased sediment permeability of sub-freezing mining would result in the contraction in the spread range of pressure drop and a decrease in the ultimate gas recovery (Shen et al., 2020). Guo et al. (2020) and Gao et al. (2021) both adopted the step-wise depressurization for water-saturated (water saturations of 64% and 20%–40%) hydrate-bearing sediments to reduce water production, however, the final gas production efficiency was also sacrificed to some extent. The ideal depressurization method should be to enhance gas production without increasing water production. Additionally, the above-mentioned studies are mostly based on a sealed environment, and there are few specific laboratory researches on the influence of peripheral fluid infiltration on hydrate exploitation. Meanwhile, simply dividing the reservoir into gas-saturated and water-saturated types cannot help fully understand the influence mechanism of pore fluids on hydrate decomposition. In our previous work, we established an unsealed water-saturated environment for hydrate exploitation simulation, and the gas-phase space was applied to the analysis of gas injection effect on the gas/water production (Sun et al., 2021). The results revealed the significance of gas-phase space in the hydrate exploitation. For the unsealed water-rich system, the infiltration of peripheral water would occupy a lot of gas-phase space and hindered gas diffusion, which further lead to CH_4 recovery decrease. The low gas production efficiency of the stage depressurization method may be due to the high saturation of pore water as well as the low decomposition driving force. Therefore, a deeper and more comprehensive knowledge of the relationship between the pore fluid and the gas-water production is very important for NGHs development. Considering the dynamic changes of pore fluid compositions in sediment with the multiphase fluid seepage (Che et al., 2015), it is necessary to further investigate the effects of different pore water saturations on hydrate decomposition and gas flow, rather than a simple classification of water-rich and gas-rich reservoirs.

These works remind us that the high-efficient establishment of gas channels and expansion of the gas-phase space in the reservoir could be crucial to improve the hydrate production efficiency. From this perspective, the spatiotemporal evolution pattern of pore fluid is critical to optimize the parameters for both depressurization and gas injection technologies. Therefore, in this work, we synthesized a series of hydrate-bearing reservoir samples with water saturation from 20% to 65% in a one-dimensional visual simulation system and focused on the influence of relatively stationary pore fluids on hydrate decomposition kinetics by top depressurization. The quantitative relationship between gas release space and gas production rate was determined. Furthermore, the gas/water production behaviors by bottom depressurization from the gas-saturated and water-saturated reservoirs were compared. The phenomena of partial hydrate decomposition and reformation with the fluid flow was found. In order to further reveal the significant influence of pore fluid composition, we explored gas/water migration and production behaviors upon the process of peripheral fluid infiltration and auxiliary gas sweep. Finally, based on this work, an optimization strategy of depressurization was put forward.

2. Experimental section

2.1. Experimental apparatus and materials

As shown in Fig. 1a, the experimental apparatus used in this work consisted of four parts: injection system, reaction system, production system and monitor and control generated system (MCGS). The injection system was applied to injecting gas and liquid into the reaction system from top and bottom, and then simulating hydrate samples with different initial saturations and occurrence environment. The reaction system was used to simulate and observe the formation and decomposition of hydrates in the sediments, and its core was a one-dimensional cylindrical reactor with an internal volume of ~0.5 L (1000 mm length, 25.4 mm diameter) and a safe operating pressure of 20 MPa. As shown in Fig. 1b, the reactor was composed of four stainless steel tubes and three sapphire tubes (100 mm length, 25.4 mm diameter) which

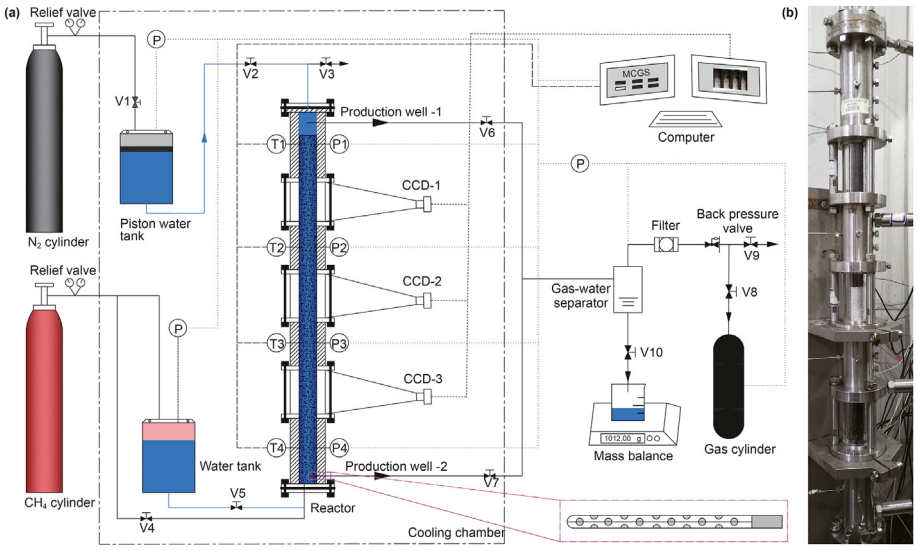

Fig. 1. Schematic of the experimental apparatus.

were alternately assembled. Specifically, stainless steel tubes were used to connect temperature and pressure sensors, while sapphire tubes were used to observe sample changes. The entire reaction system was placed in a large cooling chamber to simulate the ambient temperature of the hydrate sample. The production system was connected to the reactor through the two production wells, and its main function was to separate and collect the produced gas and water. MCGS was used to analyze and record the temperature, pressure and gas flow rate data during the experiments.

In this work, CH_4 gas and N_2 gas with a purity of 99.99 mol% were supplied by the Beijing Haipu Gas Company, Ltd. The deionized water was produced by a water distillation unit from the Shanghai Yarong Biochemistry Instrument Factory. The sodium chloride solution with a salinity of 33.5 g/L was prepared in the laboratory. The hydrate-bearing sediment samples were simulated with 20–40 mesh quartz sands.

2.2. Experimental procedure

(a) Formation of hydrate-bearing sediments

The method of preparing gas-rich hydrate-bearing sediments in this experiment was basically the same as our previous studies (Sun et al., 2021). Briefly, the preparation process of hydrate samples was strictly carried out according to the following operations to keep their properties consistent: (1) the temperature of the cooling chamber was pre-adjusted to 0.1 °C. The pre-prepared quartz sand and brine in this cooling chamber were fully mixed and tightly filled into the reactor. This method could ensure CH_4 hydrate evenly distributed in the reservoir (Wang et al., 2017b). Then the entire experimental apparatus was assembled and evacuated with a vacuum pump for 5 min. (2) Valve 4 was opened and CH_4 gas was injected into the reactor to the pressure of 10.0 MPa. The temperature of the cooling chamber was adjusted to 5.0 °C. The formation of hydrate-bearing sediments sample was considered complete until the pressure in the reactor stabilized for > 12 h, and the final pressure was ~4.6 MPa. (3) After the above operations, the hydrate saturation and the water saturation of the reservoir samples were usually ~30% and ~20%, respectively. To investigate the influence of different pore fluids, a certain amount of deionized water saturated with CH_4 at 5 °C and 4.6 MPa was injected into the reactor from the bottom at a rate of 0.5 g/s, while the squeezed CH_4 was released from the reactor top to maintain a constant reservoir pressure. Through the above operations, the hydrate-bearing sediments with the same hydrate saturation and the different gas/water saturations were prepared. The specific properties of the nine hydrate samples are listed in Table 1 and Table 2. The detailed calculation method of the saturations of gas, water and hydrate, the CH_4 recovery ratio and the hydrate decomposition ratio can be referenced in our previous work (Yuan et al., 2011; Sun et al., 2018a).

(b) Depressurization

Fig. 2 shows the schematics of the simulated hydrate-bearing reservoir samples for Runs 1–9. For Runs 1–5, the depressurization position was located at the reactor top, and an isolated space with a height of 5 cm was established to block water outflow. The volume of gas phase in the reservoir would increase slightly due to the volume shrinkage of hydrate phases during hydrate decomposition. For Runs 6–9, the depressurization position was located at the reactor bottom, and the pore water would be smoothly produced through the production well. It should be noted that a water tank with a constant pressure of 5 MPa was connected to the reactor top to simulate the peripheral water infiltration into the unsealed reservoir in Run 8, and a N_2 tank was connected to the reactor top to explore the effect of gas sweep on fluid flow and hydrate decomposition in Run 9. N_2 was injected into the reservoir at a rate of ~0.4 SLM following the depressurization. The produced

Table 1
Properties of the prepared CH_4 hydrate sediments and experimental conditions for Runs 1–5.

Runs	1	2	3	4	5
Quartz sand, mesh	20–40	20–40	20–40	20–40	20–40
Temperature[a], °C	4.6	4.6	4.7	4.7	4.7
Pressure[b], MPa	4.66	4.60	4.64	4.63	4.64
Hydrate saturation, %	29.8	29.8	30.6	29.3	29.2
Water saturation, %	21.4	29.5	44.9	55.9	65.9
Gas saturation, %	48.8	40.7	24.4	14.8	4.9
Production well number	1	1	1	1	1
Production pressure, MPa	3.7	3.7	3.7	3.7	3.7

[a] Average value of T1-T4 after hydrate formation was complete.
[b] Average value of P1–P4 after hydrate formation was complete.

Table 2
Properties of the prepared CH_4 hydrate sediments and experimental conditions for Runs 6–9.

Runs	6	7	8	9
Quartz sand, mesh	45/250	45/250	45/250	45/250
Temperature[a], °C	5.2	5	5	5.1
Pressure[b], MPa	4.53	4.61	4.62	4.60
Hydrate saturation, %	30.4	30.6	30.5	30.3
Water saturation, %	19.9	63.8	65.1	65.1
Gas saturation, %	49.7	5.6	4.4	4.6
Overlying aquifer, L	/	/	5.0	/
N_2 injection rate, SLM	/	/	/	0.4
Production well number	2	2	2	2
Production pressure, MPa	3.7	3.7	3.7	3.7

[a] Average value of T1-T4 after hydrate formation was complete.
[b] Average value of P1–P4 after hydrate formation was complete.

gas composition was analyzed by a gas chromatography (GC, Agilent 7890B) every 15 min. In addition, for all experiments, the production pressure was 3.7 MPa. During depressurization, the system temperature, pressure and water production were recorded every minute.

3. Results and discussion

In this study, a series of experiments were carried out to investigate the kinetics of hydrate decomposition and gas production from the reservoir under different pore fluid conditions by depressurization. For the first five experiments, a series of specific hydrate samples with initial water saturations of 21.4%, 29.8%, 44.9%, 55.9% and 65.9% were established to determine the relationship between gas production efficiency and pore fluid composition under a specific reservoir *p-T* condition, which is the basis of further optimizing hydrate mining technology by regulating the fluid migration behavior. The successive experiments (Runs 6–9) were then performed to explore the differences between the global and local decomposition behavior caused by multiphase fluid flow and gas-liquid redistribution in the pores. In addition, the effect of depressurization together with gas sweep on pore fluid flow and distribution was also investigated. This auxiliary gas sweep presented a significant advantage on the rapid production of pore water, and showed great application potential in water-saturated hydrate production.

3.1. The effect of water saturation on hydrate decomposition

An overview of the hydrate decomposition kinetics experiments (Runs 1–5) is shown in Fig. 3. Through strict controlling of the hydrate synthesis process, the only difference of the five reservoir samples in experiments was the initial gas-water saturation. The depressurization-induced driving force for hydrate decomposition in Runs 1–5 was almost constant in the early stages. When the decomposition ratios exceeded 20%, the influence of pore water content on the hydrate decomposition gradually became prominent. The gas transfer resistance was relatively lower at lower water saturation because of the gas connection in the pores. On the other hand, high water content in reservoir would undoubtedly hinder gas bubble formation and transfer. The effect of water acting as a diffusion barrier of decomposed gas has also been observed through high resolution CT technique (Yang et al., 2016). The additional pressure in the pores caused by capillarity further reduced the driving force for hydrate decomposition. Especially when the reservoir pressure decreased to the production pressure, it was more difficult to form large enough bubbles at the interface between hydrate and methane-saturated water without pressure drive. As a result, the elapsed times of CH_4 hydrate complete decomposition in Runs 1–5 were 275, 310, 482, 787 and 1000 min, respectively. Hydrate decomposition and gas production were positively correlated, considering more gas released from high-efficient hydrate decomposition. As shown in Fig. 3b, the average CH_4 production rates of hydrate complete decomposition were 0.063, 0.054, 0.030, 0.017 and 0.012 L/min, respectively. Obviously, the lower the water saturation of the reservoir, the higher the gas production rate. It should be pointed out that the hydrate decomposition and gas production were mutually supporting, which jointly determined the efficiency of hydrate exploitation. The excess pore water not only inhibited the hydrate decomposition, but also hindered the gas transfer.

During the process of depressurization-induced hydrate decomposition, hydrate was converted into gas and water. For Runs 1–5, the water saturation in the reservoir changed greatly because the water from hydrate decomposition accumulated while almost no drainage during the whole process. By contrast, the change of gas saturation in the reservoir was relatively low. As shown in Fig. 3c, the small increases of gas saturation in the reservoir in each run were caused by the volume difference of the CH_4 hydrate and water before and after decomposition. As a result, the corresponding gas-phase space in the reservoir would increase slightly, and the expanded volume was related to the amount of hydrate decomposition. Considering the relatively consistent gas saturation, we averaged the gas saturation of the reservoir before and after depressurization and then correlated the average values with

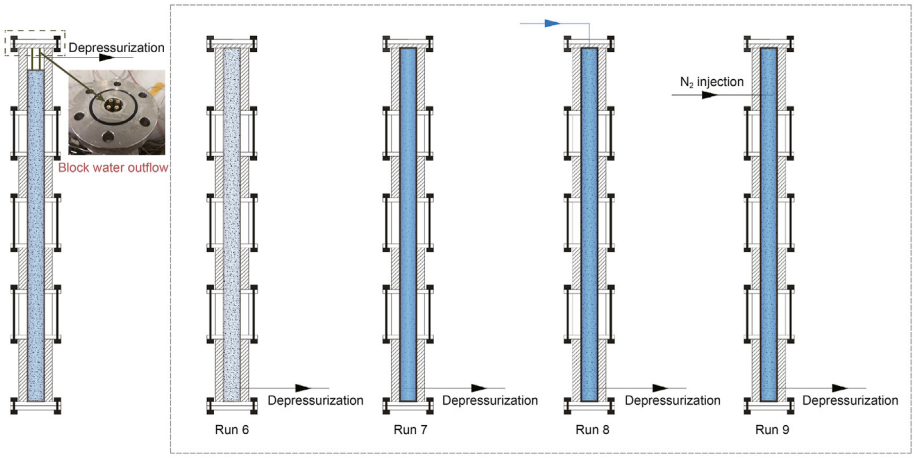

Fig. 2. Schematics of hydrate sample for Runs 1–9.

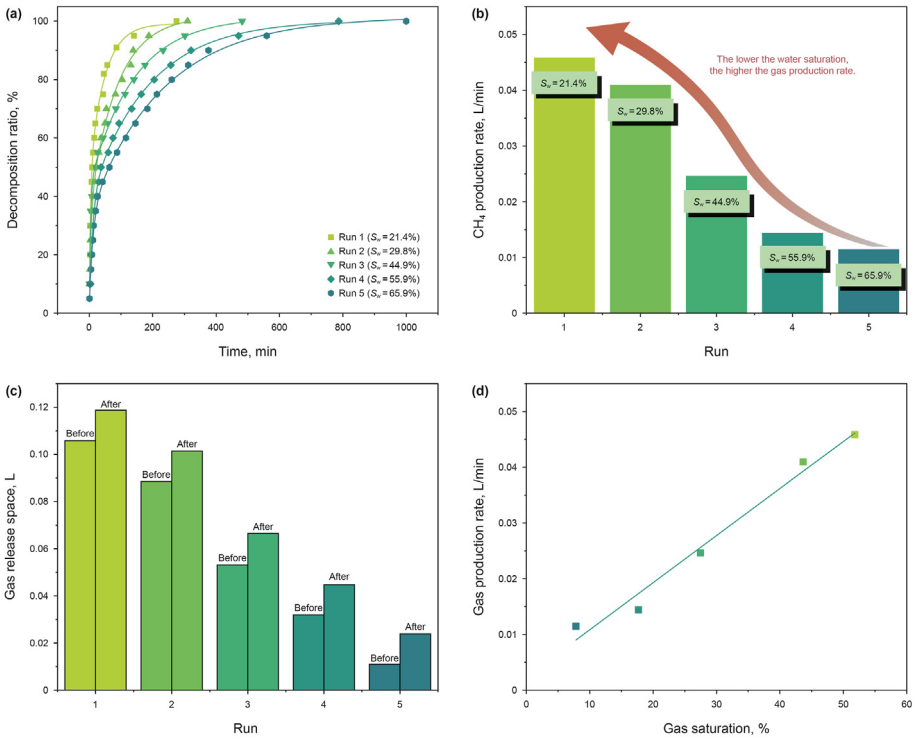

Fig. 3. The results of CH_4 hydrate decomposition and gas production in "water-locked" environment by depressurization method. (**a**) The variations of hydrate decomposition ratio over time until complete decomposition. (**b**) Comparison of the average CH_4 production rate. (**c**) Volumes of gas release space before depressurization and after hydrate complete decomposition. (**d**) Linear relationships between the average gas saturation in reservoir and average gas production rate at the experiment conditions.

the average gas production rates of each run. As shown in Fig. 3d, the result revealed a linear relationship between the gas saturation (~20%–50%) and the gas production rate with a slope of 8.4×10^{-4} L min^{-1}/%. Notably, roughly for every 10% increase in gas saturation, the gas production rate could be doubled. Therefore, although there are other factors influencing the practical process of hydrate exploitation, expanding the gas-phase space is to be one of the most effective ways for improving the gas production efficiency. From this point of view, the improvement strategy of the production efficiency and gas-water ratio should not reduce water production at the expense of gas production, but increase the gas space in the reservoir as soon as possible in the early stage and maintain the gas space during the whole depressurization process. This may lead to a lower gas-water ratio in the early stage, but it is extremely beneficial to the entire gas production.

3.2. Effect of pore water migration on gas production

Following the completion of "water-locked" hydrate decomposition experiments, a series of gas-water co-flow and production experiments were performed to further explore the unique relationship between gas-phase space and hydrate decomposition. Runs 6 and 7 were processed upon the bottom production well in a conventional sealed environment. On this basis, Run 8 added the simulation of the peripheral water infiltration into the reservoir, and Run 9 added an auxiliary gas sweep process. The quantitative analysis results of hydrate decomposition and gas production behaviors are shown in Fig. 4.

The primary indicators for evaluating production methods are gas production rate and gas production amount (or gas recovery ratio). As shown in Fig. 4a, the final gas recovery ratios for Runs 6–9 were 57.3, 70.6, 85.4 and 93.0%, respectively, while the corresponding average CH_4 production rates were 0.062, 0.035, 0.024 and 0.086 L/min, respectively. The results revealed that the higher gas production rate corresponds to lower gas recovery ratio in the absence of gas sweep. The reason for this phenomenon was that a large amount of gas had been left in the reservoir with the larger gas-phase space after gas production. As shown in Fig. 4b, compared with the results of Runs 1–5, there were huge expansions in the gas-phase space after the depressurization in this series of experiments. The initial free water or the water from hydrate decomposition in the pores flowed out of the reactor rapidly with the gas flow, which continuously increased the gas-phase space in the reservoir. The final obtained gas-phase spaces were 0.173, 0.147, 0.094 and 0.174 L, respectively. Under the same production pressure, although the larger gas-phase space could promote hydrate decomposition, more CH_4 gas remained in the reservoir after depressurization. From this point of view, the infiltration of the peripheral water played a role of displacing the trapped gas, thus increasing the gas production ratio. Auxiliary N_2 sweep had a more significant effectiveness on expanding gas-phase space and enhancing gas production efficiency. The main reason was that the injected gas accelerated the production of pore fluids (including water and CH_4 gas), and the presence of N_2 reduces the partial pressure of CH_4 in the pores, which could dramatically increase the driving force for CH_4 hydrate decomposition (Zhong et al., 2020). Additionally, the corresponding increases of the gas-phase spaces for Runs 6–9 were 0.054, 0.134, 0.083 and 0.164 L, respectively. Unlike the case in Runs 1–5, the main reason for the gas-phase space expansion in Runs 6–9 was the water outflow. The rapid release of pore fluid was definitely beneficial to the hydrate decomposition. The detailed water production for Runs 6–9 are shown in Fig. 4c. In Run 8, the peripheral water continuously infiltrated into the reservoir and filled the gas-phase space up, so despite the ultrahigh water production obtained, the gas-phase space volume was the lowest in Runs 6–9. Moreover, under high-permeability deposits conditions, the peripheral water invading has a fatal impact on hydrate exploitation, resulting in an extremely

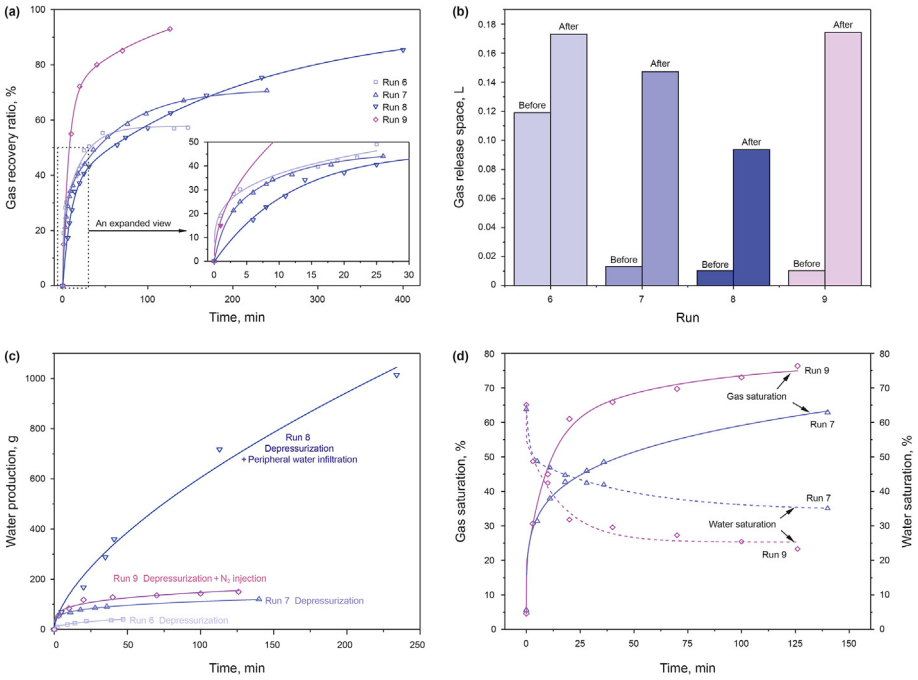

Fig. 4. (**a**) Variations of the CH_4 recovery ratios for Runs 6–9. An expanded view in the first 30 min is shown on the right. (**b**) Volumes of gas-phase space before depressurization and after hydrate complete decomposition. (**c**) Water productions during hydrate exploitation by depressurization for Runs 6–9. (**d**) Comparison of the gas saturation and water saturation between Runs 7 and 9.

low gas-water ratio and severe shrinkage of the mining area (Sun et al., 2021). In contrast, the reservoir was in a gas-rich environment for Run 6, so the water production and the increase of gas-phase space were both the lowest. Comparing the other two sets of experiments (Runs 7 and 9) in the water-rich environment without peripheral water, N_2 sweep accelerated the production of pore water, and finally obtained more gas-phase space and gas flow channels. However, the introduction of N_2 will lead to a decrease in the quality of the produced gas, resulting in an increase in the cost of subsequent gas treatment. Additionally, long-term N_2 injection also increases injection costs. It is worth noting that most of pore water was produced in the initial stage of depressurization. As shown in Fig. 4d, the changing trajectories of gas saturation and water saturation in the reservoir tend to be flat after ~25 min. After that, the effect of N_2 sweep on reducing the water saturation of the reservoir became insignificant. Therefore, we can take advantage of N_2 sweep as a springboard to enhance the water production in the early stage for establishing a large gas-phase space, and after that stop N_2 sweep to prevent from quality decrease of the produced gas. From this point of view, we can stop N_2 sweep when the water production rate drops significantly (at 25 min in this experiment), which corresponds to 0.446 mol of N_2 injected in Run 9. It should be noted that the effect of N_2 sweep on displacing pore water was initially discovered. Systematic investigation of the application of N_2 sweep in marine NGHs development and optimization of key injection parameters will be the focus of future work. Additionally, from the thermodynamic point of view, under the same pressure conditions, the hydrate equilibrium pressure corresponding to the mixture gas of N_2 and CH_4 is higher, which in turn increase the driving force for the decomposition of CH_4 hydrate (Zhong et al., 2020).

3.3. Partial decomposition and reformation behavior of CH_4 hydrate

The above experimental results reveal the important role of gas-phase space for hydrate exploitation from a macro perspective. The pore water outflow could effectively release the gas-phase space, and further accelerate hydrate decomposition. However, with the water migration to the production well, the spatiotemporal variation of gas-phase distribution in the reservoir would lead to spatial differences in hydrate decomposition and reformation along the fluid flow direction. Based on the analysis of holistic water production behavior, the main evolution of water saturation occurred within the first 25 min of depressurization, so these spatial differences mainly appeared in the early stage of mining. In Run 6, the hydrate sample was initially of high gas saturation, so the partial hydrate decomposition phenomenon at each height was consistent. In Run 7, the hydrate sample was in a typical sealed water-saturated environment, and the partial hydrate decomposition difference caused by the fluid phase migration was relatively obvious. Runs 8 and 9 further explored the influence of the peripheral water infiltration and gas sweep on the hydrates decomposition, respectively.

As shown in Fig. 5a, comparing the hydrate distribution morphology in sapphire tubes at the three different heights in Run 7, CH_4 hydrate close to the wall of sapphire tubes 1 and 2 almost disappeared at 4 min, while a lot of bubbles continuously presented in sapphire tube 3. At this time, there was a huge amount of CH_4 hydrate still remained in the reservoir from the overall gas production curve (Fig. 3a), which might be due to the better fluidity near the wall that resulted in a higher decomposition rate. With the continuous downward flow of pore water, the water saturation of the upper zone was relatively lower, which would accelerate the partial hydrate decomposition. As shown in Fig. 5b, the corresponding rapid decomposition (T1 zone) induced a drastic temperature drop. The reservoir temperature usually decreased to the hydrate equilibrium temperature corresponding to the production pressure (Falser et al., 2012). By contrast, the temperature drop in T2 zone was relatively gentle, and there was an abnormal uplift in T3 zone. These temperature variations were caused by the different hydrate decomposition and reformation behaviors in the respective spatial zones. Especially, the abnormal temperature bulge in T3 zone indicated that there were more reformed hydrates than decomposed hydrates locally. We

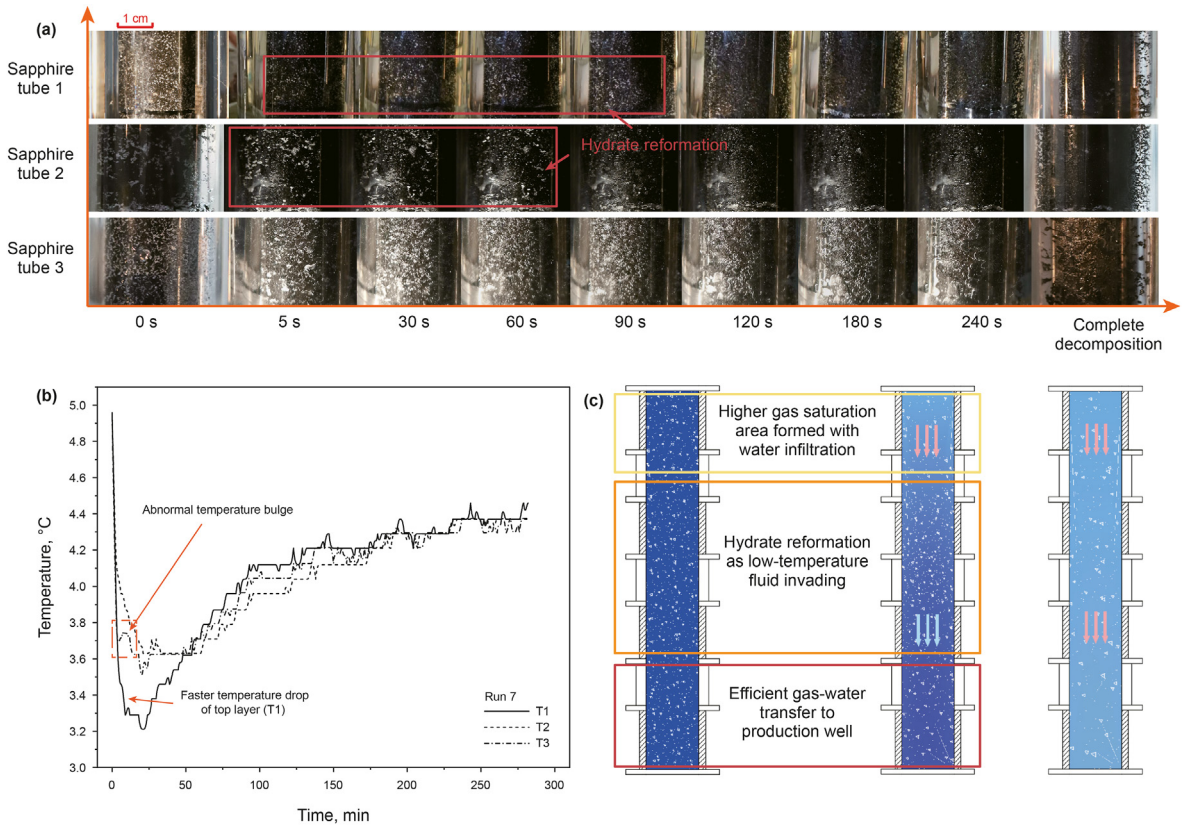

Fig. 5. The partial decomposition and reformation behavior of CH_4 hydrate in Run 7. (**a**) Observation images of reservoir evolution at different positions after depressurization. The red frame is to highlight the hydrate reformation areas. (**b**) Variations of temperatures T1-T3 after depressurization for Run 7. (**c**) Schematic diagram of the partial difference of hydrate decomposition due to pore-water migration.

also observed the secondary formation behavior of hydrate through the sapphire tubes, as shown in the red wireframe marked in Fig. 5a (CH_4 hydrate reformation process in sapphire tube 2 is shown in Video S1). The hydrate decomposition in the upper layer was faster than that in the middle region, and there were conversions between kinetic energy and pressure potential energy during the top-down flow of cryogenic fluid. Hydrate reformation could occur in channels with high pressure potential energy. Since the driving force of hydrate reformation is relatively small, we believe that this hydrate reformation is related to the memory effect (Wang et al., 2017; Kou et al., 2022), which is conducive to the hydrate regeneration behavior (Sun et al., 2020). The difference in fluidity and heat transfer caused more apparent hydrate reformation inside the reactor. For the practical production, hydrate reformation would lead to decreased permeability (Wu et al., 2020), which would in turn cause shrinkage in depressurization area as well as gas production efficiency. The characteristic of partial hydrate decomposition is shown in Fig. 5c. In the early stage of depressurization, due to the water downward migration, the upper gas-phase space increased and thus stimulated high-efficient hydrate decomposition. By contrast, affected by the high water saturation and secondary hydrate formation, the middle layer was corresponding to the lowest hydrate decomposition efficiency. Gas and liquid adjacent to the production well would be preferentially produced, so the hydrate decomposition in the lower layer was also relatively fast. When most free water was discharged from the reservoir, the hydrate could maintain a relatively high decomposition rate in a gas-rich reservoir.

In Section 3.2, we have discussed the impact of peripheral water infiltration on the decomposition and production of CH_4 hydrate. Here, in terms of the spatial effect, it was found that the water intrusion into the reservoir top might inhibit the “top advantage” of hydrate decomposition. As shown in Fig. 6a (Run 8), since the infiltrated water at the initial temperature of the reservoir (5 °C) brought heat into the reservoir, the upper temperature remained at 4.5 °C after a short convexity. In comparison, the greater temperature drop of T3 indicated faster decomposition of hydrate around the production well. The effects of reservoir temperature rise and pore water increase on hydrate decomposition were opposite. From the perspective of decomposition rate, the increase in driving force of hydrate decomposition brought by temperature rise was offset by the hindrance of fluid flow caused by pore water. Additionally, through observing the fluid flow state through the sapphire tubes (Fig. 6b), it was found that the gas bubbles that generated in the pores flowed downwards with the water in sapphire tubes 1 and 2, and extending bubbles (bubbles connected together) did not appear in sapphire tube 3 until ~90 s. After the infiltrated water and discharged water reached dynamic equilibrium, the gas saturation of the reservoir increased from 4.4% to ~40%. Nevertheless, compared with the static water-flooded state, water flooding could improve the gas production efficiency to a certain extent. For Run 9, a violent flow soon appeared in the entire reservoir due to N_2 disturbance. The morphologies in the three sapphire tubes with N_2 sweep at 30 s are shown in Fig. 6d, in which the dotted lines outline the routes of the connected bubbles that moving downwards quickly. There were always several arterial roads formed by the connected bubbles for pooled fluid flow, and CH_4 gas produced in the nearby pores was rapidly converged and brought out. Correspondingly, it can be seen from the temperature change that the hydrate had undergone more fierce decomposition, as shown in Fig. 6c. Under the same pressure, the phase equilibrium temperature of CH_4/N_2 mixed gas is lower than that of pure CH_4 (Zhong et al., 2020), which resulted a greater driving force for CH_4

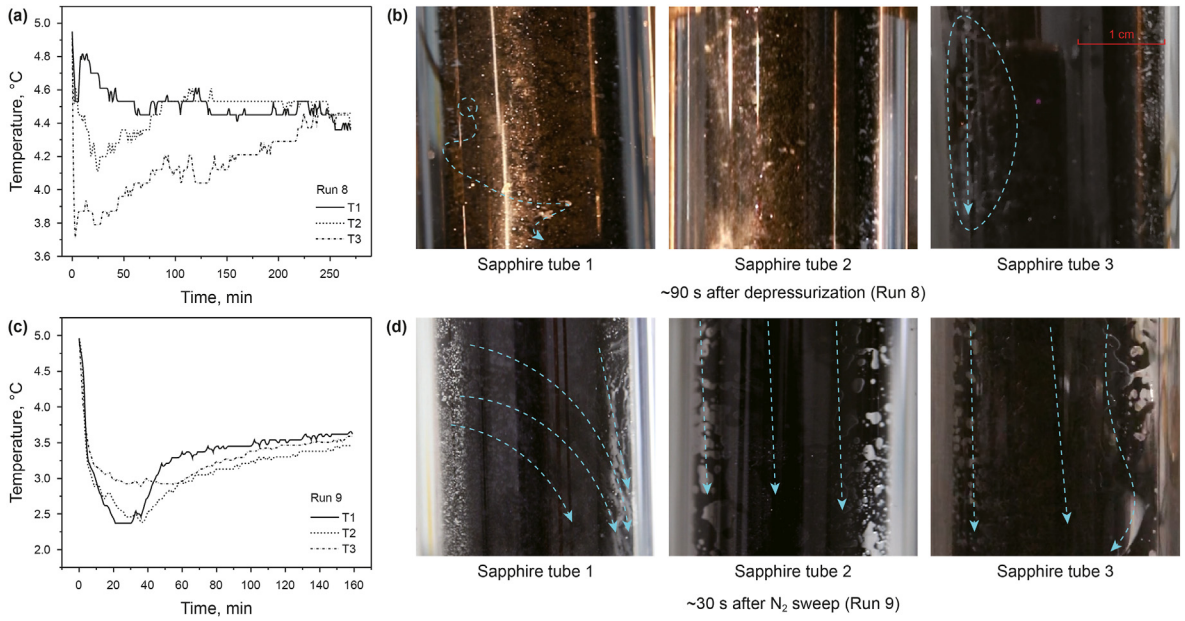

Fig. 6. (**a**) Variations of temperatures T1-T3 after depressurization for Run 8. (**b**) Observation images of reservoir pattern after depressurization for Run 8. (**c**) Variations of temperatures T1-T3 after depressurization for Run 9. (**d**) Observation images of reservoir pattern after depressurization for Run 9. The dashed lines are to depict the main gas channels for Runs 8 and 9.

hydrate decomposition. Therefore, the reservoir temperature could drop to ~2.4 °C, which was far lower than the equilibrium temperature of pure CH_4 hydrate of ~3.6 °C at the production pressure. Another notable advantage was that N_2 effectively prevented the secondary formation of hydrate, which is an urgent problem in the actual production process.

In summary, the results of the partial decomposition and reformation behavior of CH_4 hydrate proved the importance of gas-phase space for hydrate production once again. In a sealed system, the pore fluid evolution process could cause spatial difference of hydrate decomposition, and even the hydrate reformation. For the unsealed system, the pore water became a continuous phase, and hydrate decomposed faster near production well. Gas sweep was an effective means to rapidly expand the gas-phase space to enhance the hydrate decomposition as well as the gas production. Meanwhile, the effectiveness of gas injection technology in inhibiting peripheral fluid infiltration in the unsealed system had been proven in our previous work (Sun et al., 2021). In this work, our proposal is to add a short-term N_2 sweep process in the early stage of depressurization in order to quickly obtain a larger gas-phase space. When the gas-phase space in the reservoir reaches stable, N_2 sweep can be shut down to ensure the quality of produced gas. Considering that this is just a preliminary exploration, we will systematically investigate the influence of key parameters of N_2 sweep and optimize the injection conditions in the future.

4. Conclusions

In this work, we have conducted a series of experiments on the impact of pore fluid on hydrate exploitation by depressurization in a visible one-dimensional device. High-definition digital cameras were used to record the morphological change of the overall reservoir. The top depressurization was applied in the first five experiments to prevent pore water production. The results revealed a significant relationship between the gas-phase space and gas production efficiency. Accumulated pore water not only inhibited the hydrate decomposition, but also severely hindered gas flow in the pores. When the initial water saturation was in the range of 20%–65%, the gas saturation and the average gas production rate showed a linear relationship. It suggests that the gas production rate could be doubled for every 10% increase in gas saturation.

Extending on the relatively constant gas saturation, we have further investigated the effect of pore fluid flow in the reservoir on hydrate decomposition and gas/water production. The results indicated that the water released from the reservoir would effectively improve production efficiency due to the expanded gas-phase space. Meanwhile, with the water migration toward the production well, the spatiotemporal variation of gas-phase distribution in the reservoir would lead to spatial differences in hydrate decomposition and reformation along the fluid flow direction. This unique spatial difference of phase transition may lead to mining efficiency reduction. On the other hand, for the unsealed reservoir, the peripheral water infiltration caused a relatively high water saturation, which reduced the overall production efficiency and induced more water production. The auxiliary means of N_2 sweep realized the high-efficient water displacement and higher driving force for hydrate decomposition. Meanwhile, the fast-formed gas channels in the reservoir ensured the continuous high gas production rate. Considering the change trend of gas-phase space during N_2 sweep, we recommend applying gas sweep only in the early stage of depressurization to prevent from reducing the produced gas quality. Finally, these findings are of significance for the optimization of depressurization and gas injection technologies.

Acknowledgements

This work was financially supported by the National Natural Science Foundation of China, China (Nos. 52004136, 22127812, U20B6005), China Postdoctoral Science Foundation, China (Nos. 2020M670347, 2021T140382) and Guangdong MEPP Fund (No. GDNRC[2021]055).

Appendix A. Supplementary data

Supplementary data related to this article can be found at https://doi.org/10.1016/j.petsci.2022.09.015.

References

Aghajari, H., Moghaddam, M.H., Zallaghi, M., 2019. Study of effective parameters for enhancement of methane gas production from natural gas hydrate reservoirs. Green. Energy. Environ. 4, 453–469. https://doi.org/10.1016/j.gee.2018.04.002.

Boswell, R., Collett, T.S., 2011. Current perspectives on gas hydrate resources. Energy Environ. Sci. 4, 1206. https://doi.org/10.1039/C0EE00203H.

Cha, M., Shin, K., Kim, J., Chang, D., Seo, Y., Lee, H., Kang, S.P., 2013. Thermodynamic and kinetic hydrate inhibition performance of aqueous ethylene glycol solutions for natural gas. Chem. Eng. Sci. 99, 184–190. https://doi.org/10.1016/j.ces.2013.05.060.

Che, W., Liang, H., Sun, G., Su, X., Lv, L., 2015. Simulation study on the seepage characteristics of natural gas hydrate sediment. Chem. Ind. Eng. Prog. 34, 1576–1581. https://doi.org/10.16085/j.issn.1000-6613.2015.06.012 (in Chinese).

Chen, L., Feng, Y., Okajima, J., Komiya, A., Maruyama, S., 2018. Production behavior and numerical analysis for 2017 methane hydrate extraction test of Shenhu, South China Sea. J. Nat. Gas Sci. Eng. 53, 55–66. https://doi.org/10.1016/j.jngse.2018.02.029.

Chong, Z.R., Yang, S.H.B., Babu, P., Linga, P., Li, X.S., 2016. Review of natural gas hydrates as an energy resource: prospects and challenges. Appl. Energy 162, 1633–1652. https://doi.org/10.1016/j.apenergy.2014.12.061.

Chong, Z.R., Yin, Z., Tan, J.H.C., Linga, P., 2017. Experimental investigations on energy recovery from water-saturated hydrate bearing sediments via depressurization approach. Appl. Energy 204, 1513–1525. https://doi.org/10.1016/j.apenergy.2017.04.031.

Cui, J., Sun, Z., Wang, X., Yu, B., Leng, S., Chen, G., Sun, C., 2019. Fundamental mechanisms and phenomena of clathrate hydrate nucleation. Chin. J. Chem. Eng. 27, 2014–2025. https://doi.org/10.1016/j.cjche.2018.12.016.

Dallimore, S.R., Collett, T.S., Taylor, A.E., Weber, U.M., Chandra, A., Mroz, T.H., Caddel, E.M., Inoue, T., 2005. Scientific Results from the Mallik 2002 Gas Hydrate Production Research Well Program, Mackenzie Delta, Northwest Territories, Canada: Preface. Bulletin of the Geological Survey of Canada.

Dou, B., Jiang, G.S., Qin, M.J., Wu, X., Gao, H., 2009. Hydraulic mining technology used for exploitation of marine gas hydrates. Geol. Prospect. 45, 427–430 (in Chinese).

Falser, S., Uchida, S., Palmer, A.C., Soga, K., Tan, T.S., 2012. Increased gas production from hydrates by combining depressurization with heating of the wellbore. Energy Fuel. 26, 6259–6267. https://doi.org/10.1021/ef3010652.

Feng, J.C., Wang, Y., Li, X.S., 2016. Hydrate dissociation induced by depressurization in conjunction with warm brine stimulation in cubic hydrate simulator with silica sand. Appl. Energy 174, 181–191. https://doi.org/10.1016/j.apenergy.2016.04.090.

Gao, Q., Yin, Z., Zhao, J., Yang, D., Linga, P., 2021. Tuning the fluid production behaviour of hydrate-bearing sediments by multi-stage depressurization. Chem. Eng. J. 406, 127174. https://doi.org/10.1016/j.cej.2020.127174.

Guo, X., Xu, L., Wang, B., Sun, L., Liu, Y., Wei, R., Yang, L., Zhao, J., 2020. Optimized gas and water production from water-saturated hydrate-bearing sediment through step-wise depressurization combined with thermal stimulation. Appl. Energy 276, 115438. https://doi.org/10.1016/j.apenergy.2020.115438.

Hu, G., Li, C., Ye, Y., Liu, C., Zhang, J., Diao, S., 2014. Observation of gas hydrate distribution in sediment pore space. Chin. J. Geophys. 57, 1675–1682. https://doi.org/10.6038/cjg20140530 (in Chinese).

Konno, Y., Fujii, T., Sato, A., Akamine, K., Naiki, K., Masuda, Y., Yamamoto, K., Nagao, J., 2017. Key findings of the world's first offshore methane hydrate production test off the coast of Japan: toward future commercial production. Energy Fuel. 31, 2607–2616. https://doi.org/10.1021/acs.energyfuels.6b03143.

Konno, Y., Masuda, Y., Akamine, K., Naiki, M., Nagao, J., 2016. Sustainable gas production from methane hydrate reservoirs by the cyclic depressurization method. Energy Convers. Manag. 108, 439–445. https://doi.org/10.1016/j.enconman.2015.11.030.

Kou, X., Feng, J.C., Li, X.S., Wang, Y., Chen, Z.Y., 2022. Memory effect of gas hydrate: influencing factors of hydrate reformation and dissociation behaviors. Appl. Energy 306, 118015. https://doi.org/10.1016/j.apenergy.2021.118015.

Kurihara, M., Sato, A., Ouchi, H., Narita, H., Masuda, Y., Saeki, T., Fujii, T., 2009. Prediction of gas productivity from Eastern Nankai Trough methane-hydrate reservoirs. SPE Reservoir Eval. Eng. 12, 477–499. https://doi.org/10.4043/19382-MS.

Li, B., Liu, S.D., Liang, Y.P., Liu, H., 2018. The use of electrical heating for the enhancement of gas recovery from methane hydrate in porous media. Appl. Energy 227, 694–702. https://doi.org/10.1016/j.apenergy.2017.08.066.

Li, D., Ren, S., Zhang, L., Liu, Y., 2016. Dynamic behavior of hydrate dissociation for gas production via depressurization and its influencing factors. J. Petrol. Sci. Eng. 146, 552–560. https://doi.org/10.1016/j.petrol.2016.07.014.

Li, F., Yuan, Q., Li, T., Li, Z., Sun, C., Chen, G., 2019. A review: enhanced recovery of natural gas hydrate reservoirs. Chin. J. Chem. Eng. 27, 2062–2073. https://doi.org/10.1016/j.cjche.2018.11.007.

Li, X., Chen, Q., Li, G., Chen, Z., Zhang, Y., Liu, Y., 2010. The simulation of hydrate production by depressurization in deep ocean. Geosci. 24, 598–606 (in Chinese).

Makogon, Y.F., 2010. Natural gas hydrates - a promising source of energy. J. Nat. Gas Sci. Eng. 2, 49–59. https://doi.org/10.1016/j.jngse.2009.12.004.

Nair, V.C., Prasad, S.K., Kumar, R., Sangwai, J.S., 2018. Energy recovery from simulated clayey gas hydrate reservoir using depressurization by constant rate gas release, thermal stimulation and their combinations. Appl. Energy 225, 755–768. https://doi.org/10.1016/j.apenergy.2018.05.028.

Ning, F., Yu, Y., Kjelstrup, S., Vlugt, T.J.H., Glavatskiy, K., 2012. Mechanical properties of clathrate hydrates: status and perspectives. Energy Environ. Sci. 5, 6779. https://doi.org/10.1039/C2EE03435B.

Shen, S., Li, Y., Sun, X., Wang, L., Song, Y., 2020. Experimental study on the permeability of methane hydrate-bearing sediments during triaxial loading. J. Nat. Gas Sci. Eng. 82, 103510. https://doi.org/10.1016/j.jngse.2020.103510.

Sloan, E.D., 2003. Fundamental principles and applications of natural gas hydrates. Nature 426, 353–359. https://doi.org/10.1038/nature02135.

Sloan, E.D., Koh, C.A., 2007. Clathrate Hydrates of Natural Gases, third ed. CRC Press.

Sun, R., Fan, Z., Yang, L., Li, Y., Lv, X., Miao, Y., 2020. Metastable state of gas hydrate during decomposition: a novel phenomenon. Chin. J. Chem. Eng. 28, 949–954. https://doi.org/10.1016/j.cjche.2020.02.003.

Sun, Y.F., Zhong, J.R., Chen, G.J., Cao, B., Li, R., Chen, D.Y., 2021. A new approach to efficient and safe gas production from unsealed marine hydrate deposits. Appl. Energy 282, 116259. https://doi.org/10.1016/j.apenergy.2020.116259.

Sun, Y.F., Zhong, J.R., Li, R., Zhu, T., Cao, X.Y., Chen, G.J., Wang, X.H., Yang, L.Y., Sun, C.Y., 2018a. Natural gas hydrate exploitation by CO_2/H_2 continuous Injection-Production mode. Appl. Energy 226, 10–21. https://doi.org/10.1016/j.apenergy.2018.05.098.

Sun, Y.F., Zhong, J.R., Li, W.Z., Ma, Y.M., Li, R., Zhu, T., Ren, L.L., Chen, G.J., Sun, C.Y., 2018b. Methane recovery from hydrate-bearing sediments by the combination of ethylene glycol injection and depressurization. Energy Fuels 32, 7585–7594. https://doi.org/10.1021/acs.energyfuels.8b01682.

Wang, D., Wei, W., Sun, J., Peng, H., Li, C., Jia, C., Liu, C., Lu, H., 2020. Dynamic evolution of pore structures of hydrate-bearing sediments induced by step-wise depressurization. Chin. Sci. Bull. 65, 2292–2302. https://doi.org/10.1360/TB-2020-0010.

Wang, P., Yang, M., Chen, B., Zhao, Y., Zhao, J., Song, Y., 2017. Methane hydrate reformation in porous media with methane migration. Chem. Eng. Sci. 168, 344–351. https://doi.org/10.1016/j.ces.2017.04.036.

Wang, X.H., Sun, C.Y., Chen, G.J., He, Y.N., Sun, Y.F., Wang, Y.F., Li, N., Zhang, X.Y., Liu, B., Yang, L.Y., 2015. Influence of gas sweep on methane recovery from hydrate-bearing sediments. Chem. Eng. Sci. 134, 727–736. https://doi.org/10.1016/j.ces.2015.05.043.

Wang, X.H., Sun, Y.F., Wang, Y.F., Li, N., Sun, C.Y., Chen, G.J., Liu, B., Yang, L.Y., 2017. Gas production from hydrates by CH_4-CO_2/H_2 replacement. Appl. Energy 188, 305–314. https://doi.org/10.1016/j.apenergy.2016.12.021.

Wang, Y., Feng, J.C., Li, X.S., Zhang, Y., Chen, Z.Y., 2018. Fluid flow mechanisms and heat transfer characteristics of gas recovery from gas-saturated and water-saturated hydrate reservoirs. Int. J. Heat Mass Tran. 118, 1115–1127. https://doi.org/10.1016/j.ijheatmasstransfer.2017.11.081.

Wang, Y., Feng, J.C., Li, X.S., Zhang, Y., Li, G., 2016. Large scale experimental evaluation to methane hydrate dissociation below quadruple point in sandy sediment. Appl. Energy 162, 372–381. https://doi.org/10.1016/j.apenergy.2015.10.099.

Wang, Y., Li, X.S., Li, G., Zhang, Y., Li, B., Chen, Z.Y., 2013. Experimental investigation into methane hydrate production during three-dimensional thermal stimulation with five-spot well system. Appl. Energy 110, 90–97. https://doi.org/10.1016/j.apenergy.2013.04.018.

Wei, J., Yang, L., Liang, Q., Liang, J., Lu, J., Zhang, W., Zhang, X., Lu, X., 2021. Geomechanical properties of gas hydrate-bearing sediments in Shenhu area of the South China Sea. Energy Rep. 7, 8013–8020. https://doi.org/10.1016/j.egyr.2021.05.063.

Wu, Z., Liu, W., Zheng, J., Li, Y., 2020. Effect of methane hydrate dissociation and reformation on the permeability of clayey sediments. Appl. Energy 261, 114479. https://doi.org/10.1016/j.apenergy.2019.114479.

Yang, L., Falenty, A., Chaouachi, M., Haberthur, D., Kuhs, W., 2016. Synchrotron X-ray computed microtomography study on gas hydrate decomposition in a sedimentary matrix. G-cubed 17, 3717–3732. https://doi.org/10.1002/2016GC006521.

Yang, X., Sun, C.Y., Su, K.H., Yuan, Q., Li, Q.P., Chen, G.J., 2012. A three-dimensional study on the formation and dissociation of methane hydrate in porous sediment by depressurization. Energy Convers. Manag. 56, 1–7. https://doi.org/10.1016/j.enconman.2011.11.006.

Yang, X., Sun, C.Y., Yuan, Q., Ma, P.C., Chen, G.J., 2010. Experimental study on gas production from methane hydrate-bearing sand by hot-water cyclic injection. Energy Fuels 24, 5912–5920. https://doi.org/10.1021/ef100367a.

Yuan, Q., Sun, C.Y., Wang, X.H., Zeng, X.Y., Yang, X., Liu, B., Ma, Z.W., Li, Q.P., Feng, L., Chen, G.J., 2013. Experimental study of gas production from hydrate dissociation with continuous injection mode using a three-dimensional quiescent reactor. Fuel 106, 417–424. https://doi.org/10.1016/j.fuel.2012.12.044.

Yuan, Q., Sun, C.Y., Yang, X., Ma, P.C., Ma, Z.W., Li, Q.P., Chen, G.J., 2011. Gas production from methane-hydrate-bearing sands by ethylene glycol injection using a three-dimensional reactor. Energy Fuels 25, 3108–3115. https://doi.org/10.1021/ef200510e.

Yuan, Q., Sun, C.Y., Yang, X., Ma, P.C., Ma, Z.W., Liu, B., Ma, Q.L., Yang, L.Y., Chen, G.J., 2012. Recovery of methane from hydrate reservoir with gaseous carbon dioxide using a three-dimensional middle-size reactor. Energy 40, 47–58. https://doi.org/10.1016/j.energy.2012.02.043.

Zhong, J.R., Sun, Y.F., Xie, Y., Sun, C.Y., Chen, G.J., Yan, W., 2020. Effect of N_2/H_2 injection on CH_4 hydrate decomposition. Chem. Eng. J. 396, 125266. https://doi.org/10.1016/j.cej.2020.125266.

Zhou, S., Li, Q., Liu, X., Pang, W., Fu, Q., 2019. Thinking and suggestions on research direction of natural gas hydrate development. China Offshore Oil Gas 31, 1–8. https://doi.org/10.11935/j.issn.1673-1506.2019.04.001 (in Chinese).